

# An innovative probabilistic Bayesian tool to scan buried magnetised structures: testing on the Phaistos (Greece) archaeological site

S. TARANTINO<sup>1,2</sup>, R. SALONE<sup>3</sup>, L. SPAGNUOLO<sup>1</sup>, M. LA MANNA<sup>3</sup>, R. DI MAIO<sup>3</sup> AND A. EMOLO<sup>1</sup>

<sup>1</sup> *Dipartimento di Fisica "Ettore Pancini", Università degli Studi di Napoli Federico II, Napoli, Italy*

<sup>2</sup> *Istituto Nazionale di Geofisica e Vulcanologia, L'Aquila, Italy*

<sup>3</sup> *Dipartimento di Scienze della Terra, dell'Ambiente e delle Risorse, Università degli Studi di Napoli Federico II, Napoli, Italy*

(Received: 30 January 2023; accepted: 12 May 2023; published online: 20 July 2023)

**ABSTRACT** Near-surface geophysics techniques have proven their reliability in various application fields, such as geotechnical engineering, resource exploration, and archaeological research. Their success in these contexts is closely related to data interpretation methods, which must be able to resolve shallow structures/bodies that are small and/or located at short distances from each other, thus preventing their identification and discrimination due to the overlapping effects generated by different sources. Here, we propose a new data inversion tool, based on a probabilistic Bayesian approach, which is able to scan near-surface magnetised structures. The developed algorithm allows selecting the most-likely probability density function, associated with the most-likely magnetic susceptibility contrast distribution in the explored model space, by refining the discretisation of the anomalous areas, i.e. those areas corresponding to the highest susceptibility contrast. We validated the algorithm on synthetic magnetic data generated by anthropogenic-like bodies, and, then, inverted experimental magnetic measurements acquired at the archaeological site of Phaistos (Crete, Greece). In the latter case, the retrieved most-likely model fits well with the remains found in the study area, and correctly identifies the proper magnetic susceptibility contrast, thickness, and depth of the Minoan wall top brought to light by the archaeological excavation.

**Key words:** applied geophysics, magnetic data inversion, Bayesian tool, archaeological research.

## 1. Introduction

In recent decades, numerous approaches have been proposed to interpret potential-field geophysical data, such as gravimetric, magnetic, and self-potential measurements, with the aim of providing reliable estimates of the parameters characterising the sources of the observed anomalies. This requirement is all the more necessary, the higher the resolution required by the prospecting, as in the case of near-surface applied geophysics (e.g. environmental geophysics, hydro-geophysics, engineering geophysics, archaeogeophysics), which uses geophysical methods to investigate small-scale features in the shallow (tens of metres) subsurface. In particular, as concerns the interpretation of magnetic anomalies, beyond the forward modelling of buried sources (e.g. Di Maio *et al.*, 2016, 2023), several numerical methods for geophysical data inversion have been proposed. Among these, we

recall: the least-squares minimisation approach, which has been applied in the case of tiny dykes (Abdelrahman *et al.*, 2003b) or to a set of causative sources with different shapes (Abdelrahman *et al.*, 2003a); the minimum variance criterion, used for inclined dyke-like structures (Essa and Elhussein, 2019) and for idealised-geometrical bodies (Essa *et al.*, 2021); the correlation imaging method, which uses the correlation coefficient of local wavenumber of real magnetic data and transformative local wavenumber of synthetic magnetic data generated by an assumed structure to retrieve the location of the source responsible for the observed magnetic anomaly (Ma *et al.*, 2017); and the correlation similarity between the analytic signals associated with the measured magnetic anomaly and the calculated response for some geometrically simple interpretive models (Mehanee *et al.*, 2021). In addition, a broad class of numerical methods has been proposed, which are mainly based on global optimisation approaches (e.g. Asfahani and Tlas, 2007; Tlas and Asfahani, 2011; Göktürkler and Balkaya, 2012; Biswas and Acharya, 2016; Biswas, 2018; Essa and Elhussein, 2018; Di Maio *et al.*, 2020; Essa and Elhussein, 2020; Ai *et al.*, 2022; Essa and Diab, 2022) or on Bayesian strategies (e.g. Beardsmore *et al.*, 2016; Güdük *et al.*, 2021; Olierook *et al.*, 2021; Sampietro *et al.*, 2022), and are generally implemented for large-scale contexts integrating geological information as preliminary knowledge. Bayesian strategies successfully deal with under-determined problems and with not-unique solutions, i.e. when different distributions of subsurface physical parameters can adequately explain the same observed geophysical data set (Sambridge, 1999; Sambridge and Mosegaard, 2002), by introducing *a priori* constraints on the model (Parker, 1977; Sambridge and Mosegaard, 2002).

In this framework, we propose a Bayesian probabilistic approach for the inversion of magnetic data, aimed at providing a two-dimensional subsurface map, in terms of magnetic susceptibility contrast, with the goal of identifying structures at the local scale (in the order of metres) with different magnetic properties to the surrounding context (Salone *et al.*, 2022). It is an inversion method that, in a space of possible theoretical models, looks for the model that can best simulate the physical quantities measured at the surface and minimise the residuals between observed and predicted data. Indeed, the Bayesian approach differs from traditional inversion techniques (Olierook *et al.*, 2021) in that it returns the solution, in terms of *a posteriori* probability distribution, of observing a specific model among those explored. This allows us to select a specific solution through the characterisation of the posterior distribution, for instance by its mode, i.e. through the model for which the distribution attains the maximum value (e.g. Aster *et al.*, 2018). In addition, the Bayesian strategy has the advantage of naturally including any *a priori* information, if available, and easily integrating different types of data sets. This, therefore, enables the anomaly sources to be better characterised thanks to the merging of information gathered from different observables that are related to different physical quantities.

In this article, we focus on the Earth's Magnetic Field (EMF) strength data acquired in gradiometer configurations in order to reduce the long-period components of the magnetic field (due to regional and crustal effects), in the space domain, and diurnal variations, in the time domain. In fact, this data acquisition configuration enhances the short-period components of the field, which are more likely to be due to the response of shallow and small magnetic sources, such as archaeological structures, the context in which the proposed inversion method has been validated.

Magnetic properties, in the shallowest part of the subsoil, are mainly due to the presence of magnetic materials, such as magnetite, or to the thermo-remaining magnetisation, which is acquired during the cooling phase in the presence of the EMF and is associated with

anthropic materials (such as ceramics and bricks, previously fired and/or baked). However, the application of the magnetic prospection method requires some favourable conditions, since significant variations in magnetic field values can be measured only when in the presence of a clear contrast between the magnetic properties of the archaeological ruins and those of the hosting material (e.g. Piro *et al.*, 1998; Silliman *et al.*, 2000; Fassbinder, 2017, and references therein).

In designing our Bayesian tool, we were guided by the elementary principles of electromagnetic physics. In the following, first we illustrate the theoretical framework on which the proposed inversion method is based and its workflow. We, then, present the results of its application to the inversion of synthetic magnetic data to test and validate the algorithm. Finally, for further validation, the developed tool is applied to magnetic data collected at the Minoan archaeological site of Phaistos (Greece). The results, in this case, are presented and discussed in the light of the remains unearthed from an archaeological excavation based on the magnetic survey (Di Maio *et al.*, 2016).

## 2. The Bayesian algorithm

As mentioned above, the inversion algorithm presented in this paper has been developed in a Bayesian framework (Tarantola, 1987; Aster *et al.*, 2018). First, we assume that a volume of magnetic material can be represented as a set of magnetic dipoles, each of which generates its own magnetic anomaly (Telford *et al.*, 1991). If these dipoles are aligned with each other, due to the effect of induction in the presence of an external magnetic field, the whole body may exhibit residual magnetism. The volume under examination can, therefore, be considered as a continuous distribution of dipoles, resulting in a dipole moment vector per unit of volume of intensity,  $M$ , also called magnetisation intensity. Since the algorithm is based on the principle of superposition, the whole anomaly associated with the volume of magnetic material is, therefore, evaluated as the sum of the anomalies associated with the single dipoles present in the volume. Given a single dipole, whose centre is at coordinates  $(x_m, z_m)$ , the magnetic field generated at an observation point at  $(x, y)$  is:

$$F(x, z, m) = \left( \frac{m}{r^5} \right) \left[ (3\cos^2 I - 1)(x - x_m)^2 - 6(x - x_m)(z - z_m)\sin I \cos I + (3\sin^2 I - 1)(z - z_m)^2 \right] \quad (1)$$

where  $m = 2pl$  is the dipole moment ( $p$  being the magnetic charge of the dipole and  $2l$  the distance vector between the two dipole charges),  $I$  is the inclination of the magnetised dipole, and  $r$  is the distance between the dipole centre and the observation point (Telford *et al.*, 1991).

In the case of a volume of magnetic material, the dipole moment  $m(r)$ , can be replaced with magnetisation  $M(r)$ , which, for low intensity inducing fields such as the EMF, is given by:

$$M(r) = \chi F_e(r) \quad (2)$$

where  $F_e(r)$  is the EMF, and  $\chi$  the magnetic susceptibility. Therefore, Eq. 1 reads as:

$$F(x, z, \chi) = \left(\frac{\chi F_e(r)}{r^5}\right) [(3\cos^2 I - 1)(x - x_m)^2 - 6(x - x_m)(z - z_m) \sin I \cos I + (3\sin^2 I - 1)(z - z_m)^2]. \tag{3}$$

To solve the forward problem, the two-dimensional volume under study has been discretised into cells of size  $(\Delta x, \Delta z)$  along the horizontal and vertical directions, respectively, each of which is characterised by a susceptibility contrast  $\Delta\chi$  per unit of volume in the SI, which is the parameter to be explored in the inverse problem. The magnetic anomaly formula, at the observation point and corresponding to the single cell, can, then, be written as:

$$F(x, z, \Delta\chi) = \left(\frac{\Delta\chi F_e(r)\Delta V}{r^5}\right) [(3\cos^2 I - 1)(x - x_m)^2 - 6(x - x_m)(z - z_m) \sin I \cos I + (3\sin^2 I - 1)(z - z_m)^2] \tag{4}$$

where  $\Delta V$  is the volume of the elementary cell considering a unit dimension in the transverse direction, not explored here.

In the case of a magnetic survey performed in gradiometer configuration, the magnetic gradient is given by:

$$\frac{\partial F(x, z_1, z_2, \Delta\chi)}{\partial z} = \frac{F(x, z_2, \Delta\chi) - F(x, z_1, \Delta\chi)}{z_2 - z_1} \tag{5}$$

where  $z_1$  and  $z_2$  are the vertical coordinates of the two sensors. According to the principle of superposition, the magnetic gradient, at the observation point  $(x_k, z_{1k}, z_{2k})$ , can finally be written as:

$$G_k = \sum_{ij} \frac{\partial F}{\partial z} (x_k, z_{1k}, z_{2k}, \Delta\chi_{ij}) \tag{6}$$

where the sum runs over all the cells in which the explored medium has been discretised.

Once the forward problem has been solved as described above, the misfit function can be defined as:

$$misfit = \sum_k (G_k - d_k^{obs})^2 \tag{7}$$

where  $d_k^{obs}$  is the observed magnetic gradient measured at  $x_k$ , with  $k = 1, \dots, N$ , with  $N$  being the number of collected data. In the applications shown afterwards, prior information on susceptibility contrast spatial distribution (maximum ignorance *a priori*) is not included. In this case, according to the Bayes theorem, the posterior probability density function (*Ppdf*), associated with the  $\Delta\chi_{ij}$  susceptibility contrast distribution, can be defined as:

$$Ppdf \propto e^{-misfit}. \tag{8}$$

For completeness of description, if any prior information about the model were available in terms of an *a priori pdf* [ $q(\Delta\chi)$ ], the posterior *pdf* would be given by:

$$Ppdf \propto q(\Delta\chi) e^{-misfit}. \quad (9)$$

However, as mentioned above, no *a priori* information has been used for the present study. In any case, a preliminary visual inspection of the observed data allows us to set the number of magnetic susceptibility anomalies, likely to be expected for the investigated volume, and, also, the range [ $\Delta\chi_{min}, \Delta\chi_{max}$ ] of the susceptibility contrast to be explored. Then, for each given  $\Delta\chi$  distribution, consistent with the above requirements, the algorithm generates a posterior *Ppdf* function. The *Ppdf* functions are, then, normalised and sorted in descending order, from the most likely to the least likely. This means that we obtain a sequence of  $\Delta\chi$  distributions in the subsoil, sorted from the most likely to the least likely, with the associated likelihood. Next, it is possible to select several  $\Delta\chi$  maps from the most likely ones, and this enables identifying areas where magnetic susceptibility contrasts are most likely to be present. Subsequently, these areas are further discretised at a spatial step smaller than the previous one, and a new inversion is performed. At the end of this second inversion step, the final solution is identified as the most likely *a posteriori*  $\Delta\chi$  distribution map (MAP model), i.e. with the model corresponding to the maximum of the *Ppdf*. Once the MAP model is obtained, we can estimate the uncertainties associated with the susceptibility contrast, retrieved for each contrast in each cell in which the explored model has been previously discretised. Finally, a map, representing the probability of observing the magnetic contrast susceptibility value,  $\Delta\chi$ , for each cell of the MAP model (independently of the magnetic contrast values in the surrounding cells), is produced. This probability is defined as follows:

$$P_{ij} = P \left[ \Delta\chi(x_i, z_j) = \Delta\chi_{MAP}(x_i, z_j) \right]. \quad (10)$$

This marginal probability provides a measure of how well the  $\Delta\chi$  value is constrained in the MAP model, for each cell ( $i, j$ ). In other words, the higher this probability, the more constrained the susceptibility contrast retrieved in a given cell.

The uncertainty on the contrast value in each cell is, then, determined from the cumulative of the probability density function of the magnetic susceptibility contrast related to each cell. We consider uncertainty the half-width of the interval at the 68% confidence centred on the MAP model. In the following, we will indicate this uncertainty with  $\sigma_{ij}$ .

A block diagram, describing the different steps performed by the inversion algorithm, is shown in Fig. 1. Summarising, the input consists of magnetic gradiometer data collected along a given profile. The size of the explored two-dimensional subsurface section, and the dimension of the discretisation cell, can be selected by the user, while the number of expected anomalies and range of the explored susceptibility contrast are inferred from a visual inspection of the data to be inverted. After a first inversion, which is already able to locate the anomalous zones, the susceptibility contrast maps are sorted by decreasing normalised probability. A further inversion, in which the most likely maps are thinner discretised, is, then, performed. The output is given by the probability distribution associated with all the possible susceptibility contrast distributions explored. The maximum *a posteriori* one is selected as the result, and the uncertainties associated with the  $\Delta\chi$  value, obtained in each cell, are provided.

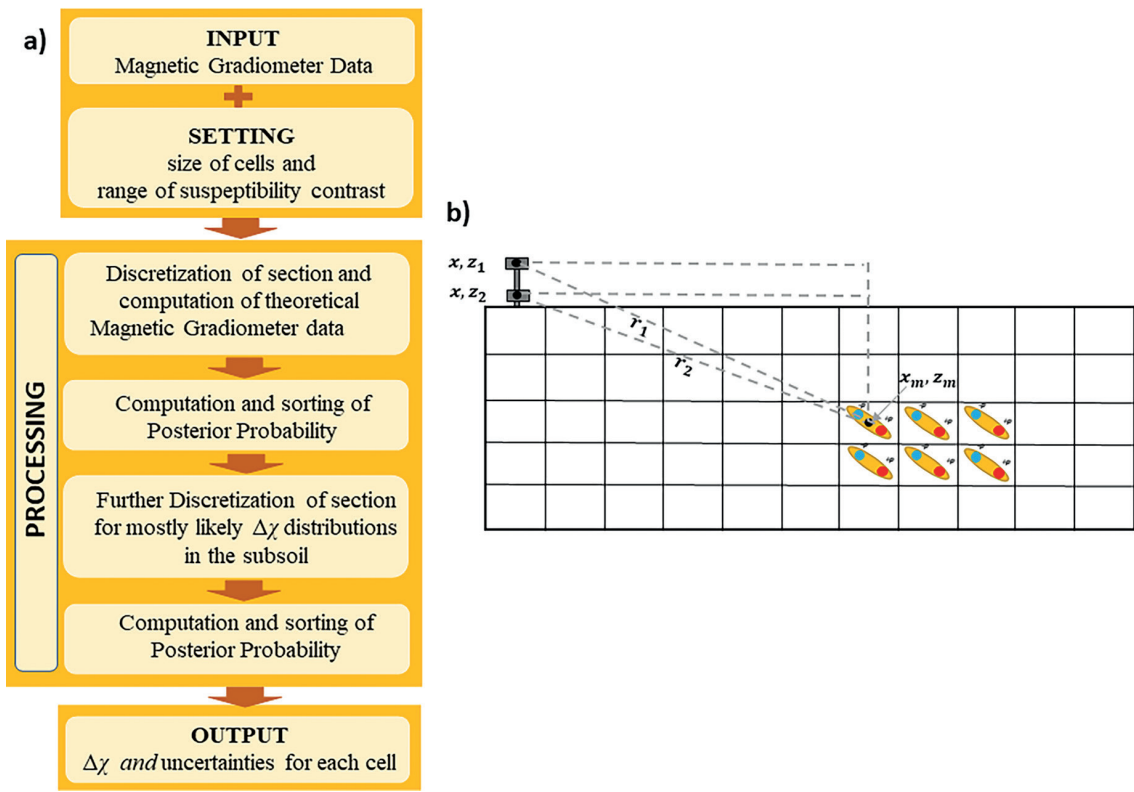


Fig. 1 - Block diagram of the inversion algorithm: a) the input requires magnetic gradiometer data, cell size, susceptibility contrast range to be explored; the processing operations are summarised in the central block; the output is the susceptibility contrast associated with the MAP model and relative uncertainties for each cell; b) sketch of the discretised medium under investigation, where  $r_1$  and  $r_2$  are the distances between the generic cell and the two sensors of the gradiometer.

### 3. Analysis of synthetic magnetic data

To verify the performance of the implemented algorithm, several tests were performed on synthetic magnetic data sets. For brevity, the results of only two representative tests are discussed here. The first test considers a structure characterised by a single magnetic susceptibility contrast, with respect to the host material, while the second one involves two separate structures, having different magnetic susceptibility contrasts, with respect to the surrounding subsoil. Given the distributions of the susceptibility contrasts, we generated the synthetic data, namely the vertical magnetic gradient values, measured in proximity of two sensors placed at a height of 1.5 m and 1 m above the surface level, along a 12 m long profile with a 0.5-m sampling step. A random noise, Gaussian distributed with zero mean and standard deviation equal to 5% of the maximum absolute value of the simulated magnetic gradient, was added to the synthetic data to imitate a realistic data set to be inverted.

The first model (Fig. 2b) consists of a 12 m long by 4 m deep section, hosting a 3 m × 1 m single structure, placed at an offset of 5 m from the origin of the section, with the top at a depth of 1.5 m from the surface level. A positive susceptibility contrast, with respect to the host material of  $\Delta\chi = 0.08$  (per unit of volume in the SI), was assumed. Synthetic data (Fig. 2a) were, then, generated as described above.

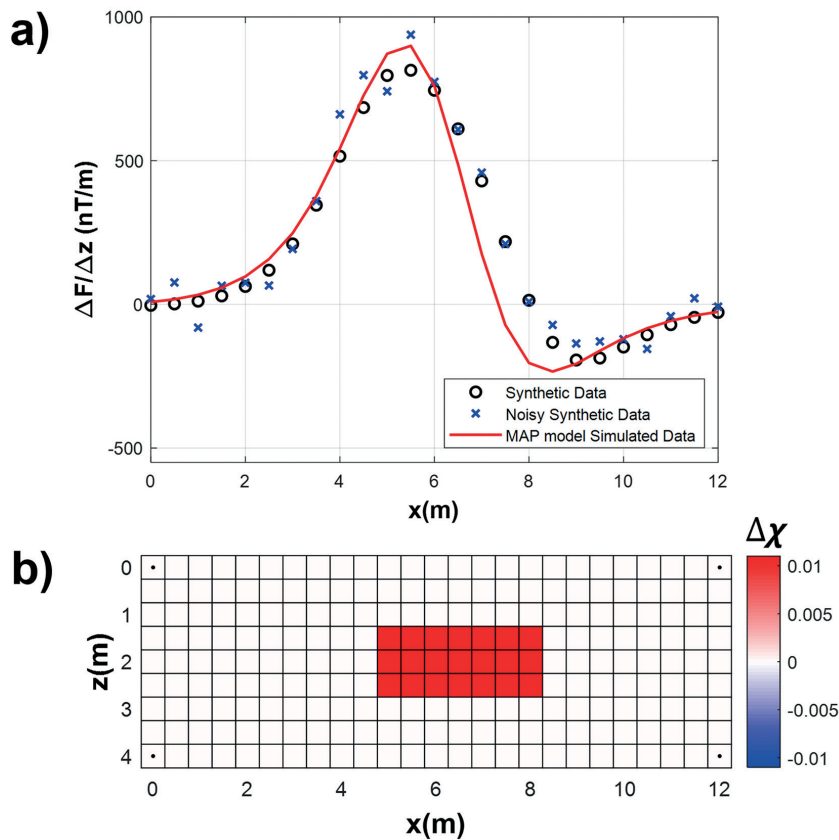


Fig. 2 - 1st synthetic test, single anomaly source: a) synthetic data (black open circles) of vertical gradient of the magnetic field associated with the model shown in panel b, noisy synthetic data with the addition of random Gaussian noise (blue crosses), and simulated data (red line) corresponding to the MAP model retrieved by the inversion procedure; b) distribution of the magnetic susceptibility contrasts,  $\Delta\chi$ , in the subsoil per unit of volume in the SI, assumed for the test, according to the colour scale shown; the black dots are plotted as a reference for the centre of the cells.

For the data inversion, we chose  $\Delta x = 2$  m and  $\Delta z = 1$  m as sampling steps along the horizontal  $x$  and vertical  $z$  directions, respectively, assuming that the magnetic susceptibility contrast varied in the range  $[0; 0.1]$ , in steps of 0.02. In the second iteration, the cells are thickened with sampling steps along the  $x$  and  $z$  directions, equal to half of the previous step, and the susceptibility contrast sampling is also assumed as equal to half of the previous one. The most likely map (MAP model) found by the inversion algorithm is shown in Fig. 3a. It reveals an anomaly of about  $2.5$  m  $\times$   $1.5$  m, characterised by susceptibility contrast values between 0.05 and 0.15 per unit volume in the SI. Size and position of the detected structure are very close to those chosen for the theoretical model, although the anomaly would seem to continue even deeper. However, examining the probability map associated with the retrieved values for each cell in the MAP model (Fig. 3b), the probabilities, related to the susceptibility contrast values for the deepest cells (depths larger than, or equal to, 3 m), are lower than those for cells located at the right depth. Moreover, the structure centre shows the highest probabilities, i.e. it is well constrained, while the probability decreases moving towards the structure edges, this being a transition zone between the anomaly source absence and presence. The susceptibility contrast reaches higher values compared to the theoretical ones at the centre, and lower values at the edges. However,

the mean value for the whole structure is very close to the one expected. The magnetic gradient, associated with the MAP model (red line in Fig. 2a), is in good agreement with the synthetic data, although the amplitude turns out to be somehow slightly greater. The misfit is of the order of  $2.2 \times 10^{-4} \frac{nT}{m}$ .

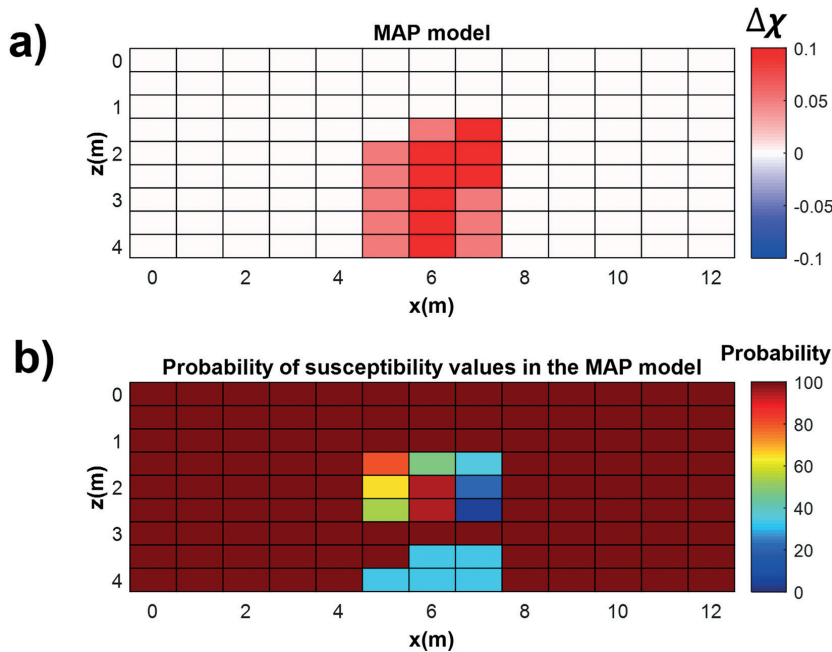


Fig. 3 - 1st synthetic test: a) MAP model retrieved from the inversion procedure: the colour scale represents the magnetic susceptibility contrast per unit of volume in the SI; b) probability map (as defined in Eq. 10) of observing, for each cell, the value provided by the MAP model.

The configuration assumed for the second test is shown in Fig. 4b. In this case, we consider a 20 m × 3 m subsurface section, hosting two 2.5 m × 1.5 m anomaly sources, placed at an offset of 5 m and 15 m, respectively, from the origin of the section, with their top at a depth of 1.5 m from the surface level. Positive magnetic susceptibility contrasts, with respect to the surrounding context equal to  $\Delta\chi = 0.008$  and  $\Delta\chi = 0.0082$  per unit volume in the SI, respectively, were chosen. The magnetic gradient values, relative to the synthetic model, are shown in Fig. 4a as black open circles, while the blue crosses indicate the noisy data obtained by adding, in this case also, Gaussian-distributed random noise to the synthetic data.

For the inversion, we selected  $\Delta x = 2$  m and  $\Delta z = 1$  m as sampling steps along the x and z directions, respectively, assuming that the magnetic susceptibility contrast varied in the interval [0; 0.01], in steps of 0.002. The most likely map found by the inversion algorithm is shown in Fig. 5a. It produced a misfit with data of about  $1.3 \times 10^{-2} \frac{nT}{m}$  (red line in Fig. 4a) attesting to good agreement between simulated and synthetic data.

From Fig. 5a, the presence of two anomalous bodies is evident: the first, on the left, is approximately 3 m × 2 m in size, has its top at a depth of 1 m below the surface level and is characterised by values of susceptibility contrast in the range [0.005; 0.01]; the second anomaly, on the right, is approximately 3 m wide, has its top at 1.5 m, and is characterised by susceptibility

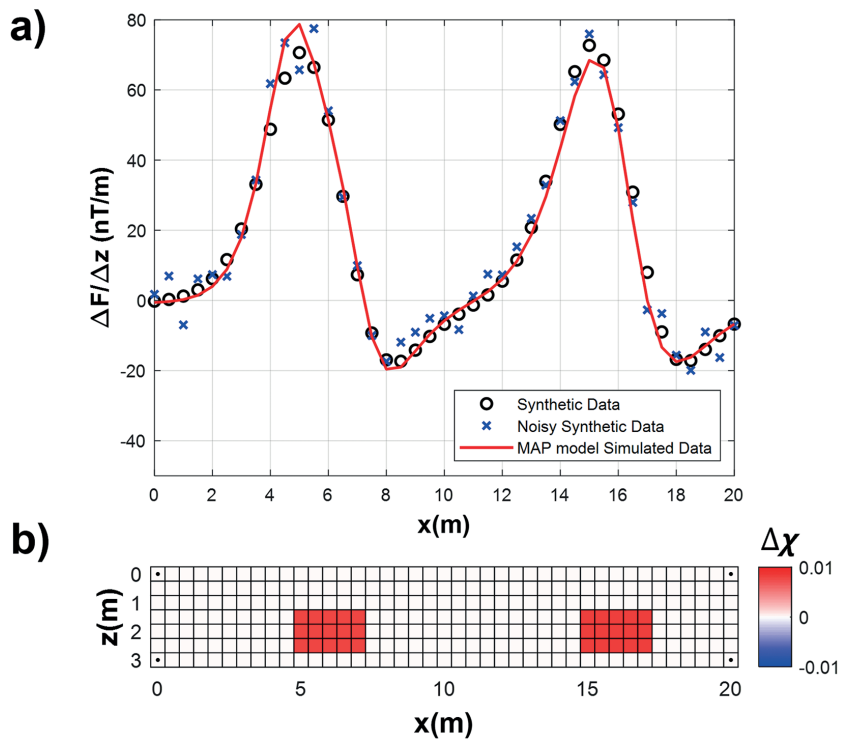


Fig. 4 - 2nd synthetic test, two anomaly sources: a) synthetic data (black open circles) of vertical gradient of the magnetic field associated with the model shown in panel b; noisy synthetic data with the addition of random Gaussian noise (blue crosses), and simulated data (red line) corresponding to the MAP model retrieved by the inversion procedure; b) distribution of the magnetic susceptibility contrasts,  $\Delta\chi$ , in the subsoil per unit of volume in the SI, assumed for the test, according to the colour scale shown; the black dots are plotted as reference for the centre of the cells.

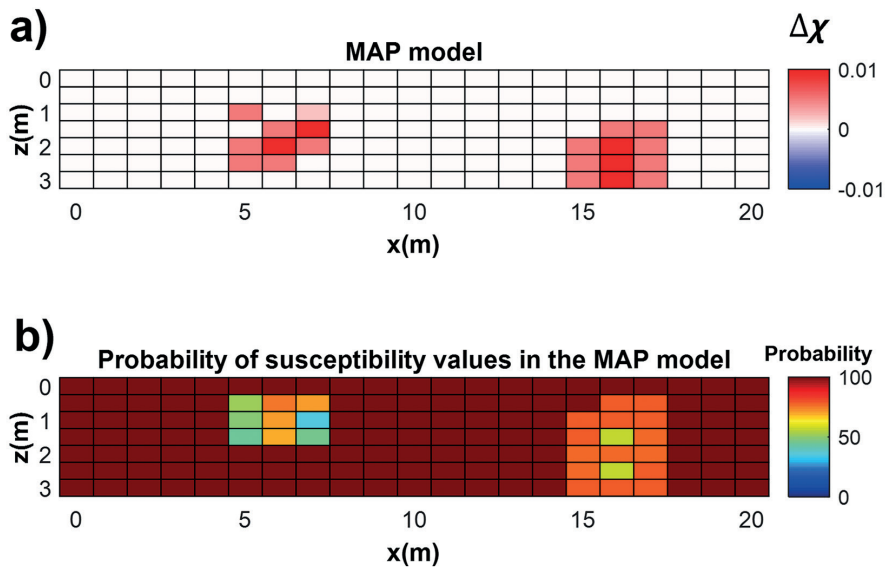


Fig. 5 - 2nd synthetic test: a) MAP model retrieved from the inversion procedure: the colour scale represents the magnetic susceptibility contrast per unit of volume in the SI; b) probability map (as defined in Eq. 10) of observing, for each cell, the value provided by the MAP model.

contrast values in the range [0.005; 0.01]. Therefore, it would seem that the inversion process is able to retrieve the true magnetic susceptibility contrast (i.e.  $\Delta\chi = 0.008$ ) between background and structures, but not a very accurate size and depth of the structures. However, by analysing the probability map (Fig. 5b) of the cells associated with the MAP model, it can be inferred that high probability values ( $\sim 90 - 100\%$ ) are associated with the cells (surrounding the anomalous sources) that are characterised by the absence of any anomalous structure ( $\Delta\chi = 0$ ). Furthermore, the offset of the two anomalies is retrieved properly. For the anomaly on the left, the cell with 1-m top is associated with a low probability value, while the cells surrounding it at the same depth do not show any contrast and, conversely, are associated with higher probability values; finally, the central cell, at a 1.5-metre depth, shows a high susceptibility contrast with a higher probability value, leading us to interpret that the top of this structure is more likely at a 1.5-metre depth. We can interpret these observations as the result of a smearing effect on the edges and a higher probability for the centre of the structure. For the body on the right side, it has its top at a depth of 1.5 m, while the susceptibility contrast values associated with its cells are higher as observed for the anomaly on the left side of the model. For this second synthetic test, similarly to the first one, the retrieved average value of the susceptibility contrast of the two bodies is very close to the true value.

#### 4. Analysis of field magnetic data

To further validate the developed Bayesian inversion tool, we applied it to field magnetic gradient data acquired by Di Maio *et al.* (2016), in the archaeological site of Phaistos (Crete, Greece) (Fig. 6a). In particular, the analysed data was extracted from the observed magnetic map along a profile (AA' in Fig. 6b) crossing a magnetic anomaly, that perfectly correlates to a calcareous wall structure brought to light by excavations guided by the results of the geophysical multimethodological survey. For details on magnetic data acquisition and the processing technique see Di Maio *et al.* (2016).

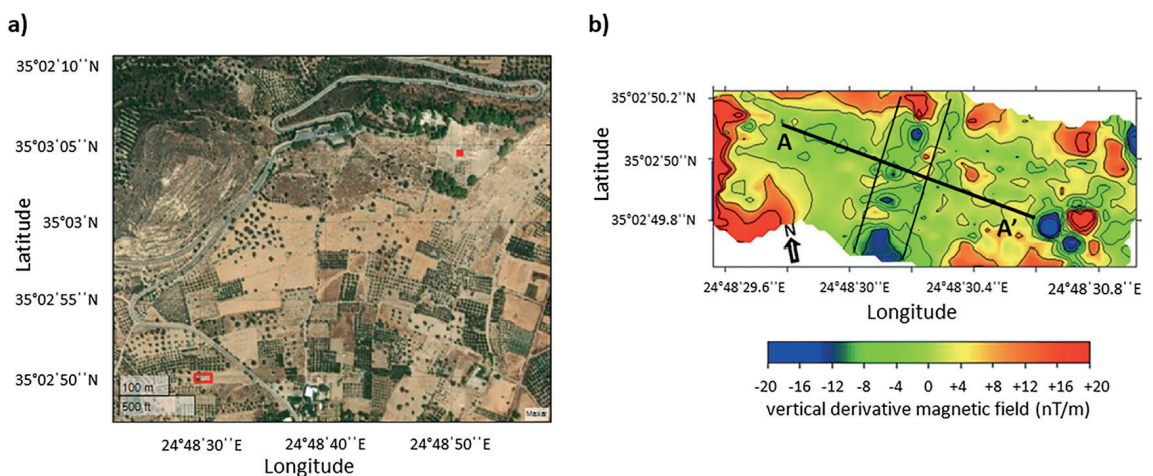


Fig. 6 - a) Geographical map of the Phaistos site (Crete, Greece). The red square in the top right corner represents the Minoan palace of Phaistos, whereas the red box in the bottom left corner delimits the area in which the magnetic survey was performed. b) Anomaly map of the vertical derivative magnetic field. Thin black continuous lines roughly indicate the boundary of a possible buried wall, while the bold black line shows profile AA' used in this study (after Di Maio *et al.*, 2016, modified).

Data, collected along the AA' profile, is shown in Fig. 7 as a blue line. Visual inspection of the anomaly pattern suggests the presence of a main anomaly with a negative magnetic susceptibility contrast with respect to the background. We investigated a 20 m × 2 m section, choosing as spatial sampling steps  $\Delta x = 2$  m and  $\Delta z = 1$  m along the horizontal and vertical directions, respectively. Moreover, we explored the susceptibility contrast  $\Delta\chi$  in the range

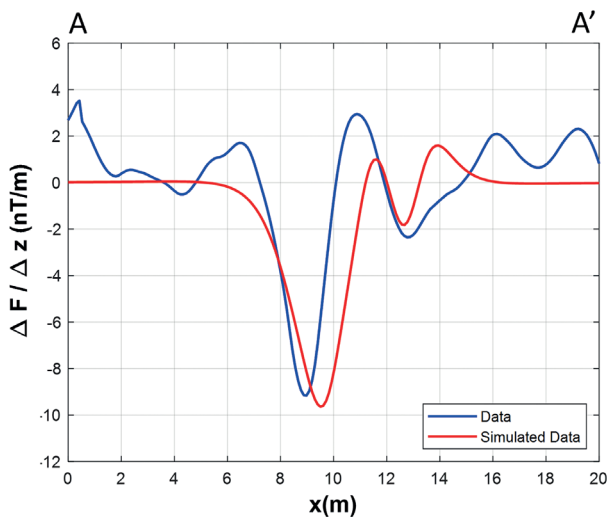


Fig. 7 - Comparison between the experimental magnetic data (blue line) along profile AA' in Fig. 6b and the simulated data (red line) corresponding to the MAP model (Fig. 8a) retrieved from the inversion procedure.

[-0.02, 0] using a step of 0.004 per unit volume in the SI. The susceptibility contrast distribution obtained from the inversion (Fig. 8a) shows the presence of a structure, about 2 m wide, located at the centre of the profile, with the top at a depth of about 1.5 m. It is characterised by a susceptibility contrast,  $\Delta\chi$ , of about -0.004 per unit of volume in the SI. On the right side of the profile, a second smaller structure is also visible at the same depth of about 1.5 m, but characterised by a lower susceptibility contrast ( $\Delta\chi \approx -0.002$  per unit of volume in the SI). The comparison between the experimental magnetic data along the profile (blue line in Fig. 7) and the simulated data (red line in Fig. 7), corresponding to the MAP model retrieved from the inversion procedure, shows that the main minimum is properly found in terms of both location and amplitude. Consistently, the probability map associated with the individual cells (Fig. 8b) shows high probability values in correspondence of the main structure identified in the MAP model, whereas lower probabilities are found for the second structure. Elsewhere, the probability values are higher, except for one cell at about 3 m offset, which corresponds to a value of the magnetic gradient larger than  $-1$  nT/m, and for which the associated error is also larger, as shown in Figs. 8b and 8c. Although the exploration for negative susceptibility contrast structures could also lead to exploring the space portion below this local minimum of the gradient (since this minimum extends along the horizontal profile for less than 1 m and has a negligible value), no structure associated with it in the MAP model was retrieved.

Location, extent and depth of the identified structure perfectly match the remains brought to light by the archaeological excavation carried out following the geophysical survey (Di Maio *et al.*, 2016), which unearthed large sectors (approximately 2 m wide) of a double-curtain fortification wall made of limestone material, at a depth of about 1.5 m from the surface level. Significantly, the remains found are chronologically consistent with historical sources on the destruction of Phaistos in 150 B.C.

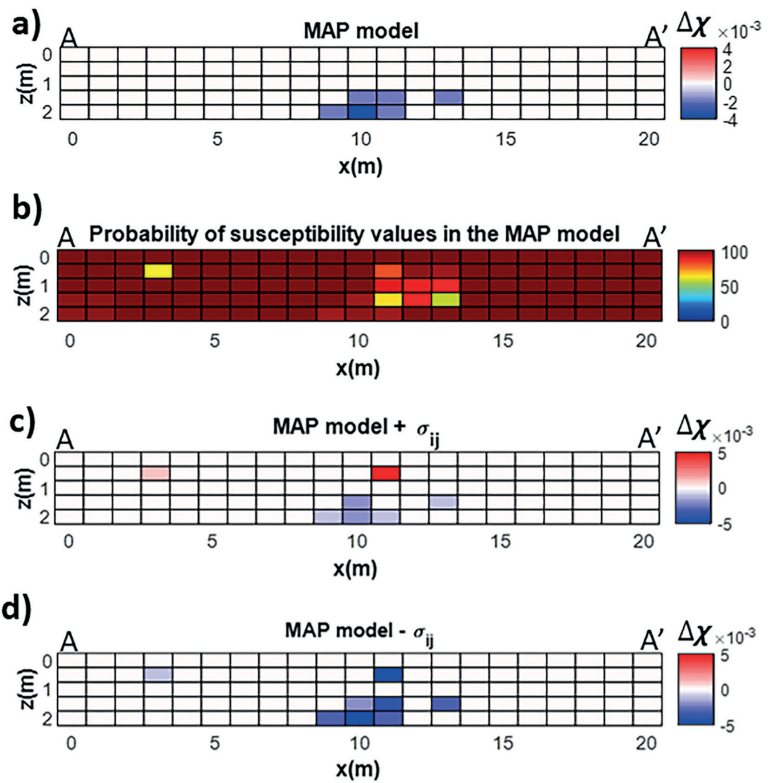


Fig. 8 - Field test: a) MAP model retrieved from the inversion procedure, the colour scale represents the magnetic susceptibility contrast per unit of volume in the SI; b) probability map (as defined in Eq. 10) of observing, for each cell, the susceptibility contrast value provided by the MAP model; c) MAP model + uncertainties ( $\Delta\chi_{ij}^{MAP} + \sigma_{ij}$ ), colour coded as in panel a; d) MAP model - uncertainties ( $\Delta\chi_{ij}^{MAP} - \sigma_{ij}$ ), colour coded as in panel a.

### 5. Conclusions

In this paper, a novel Bayesian probabilistic approach is proposed to identify buried structures characterised by different properties in terms of magnetic susceptibility contrast with respect to the host medium. The main assumption is the principle of superposition of elementary magnetic dipoles. It is, therefore, supposed that any magnetic anomaly observed at the surface, and associated with a volume of material with magnetic susceptibility different from that of the background, is due to the sum of the anomalies caused by the various single dipoles present in the volume under investigation. The possible applications of the developed inversion algorithm could be multiple. However, we highlight its usefulness for archaeological investigations, where fine characterisation of the targets (e.g. walls, tombs, etc.), in terms of location, size, and depth, is essential for properly planning any excavation project, achieving cost reduction and selecting the most appropriate methods for the excavation work.

The developed inversion tool provides, without requiring any prior geometric assumption, a solution, in terms of probability distribution, that allows the selection of the maximum *a posteriori* probability model, i.e. the model corresponding to the maximum of the posterior probability density function (Aster *et al.*, 2018). The proposed procedure also renders a complementary probability map, which represents, for each explored cell, the probability of observing the susceptibility contrast provided by the MAP model. The effectiveness of the implemented code has been validated by tests on both synthetic and field magnetic data. In particular, the test on literature field data, acquired at the archaeological site of Phaistos (Di Maio *et al.*, 2016), provided anomaly source parameters in good agreement with the characteristics of the remains unearthed in the study site.

In the future, and in order to improve our tool, we aim to find strategies to reduce smearing effects. One possible approach could be to include further data sets from other geophysical methods (e.g. gravity and geoelectrical techniques), and unify them in an integrated multi-parametric framework thanks to the probabilistic approach. In fact, the probabilistic treatment allows data of different nature to be integrated by simply defining a joint probability for the available data sets. The joint inversion would allow common features to be found and highlighted beyond the single physical properties that, analysed separately, might provide partial or weak information due to noise and/or to the under-determination and ill-posedness of the problem. In fact, a single model, able to simultaneously match all available independent data, provides a more probable solution than a model that can satisfy only a single data set (Beardsmore *et al.*, 2016). The concept is that the information, jointly revealed by different techniques, adds up constructively, better defining the position of anomalous structures with respect to the surrounding medium, while any spurious artefact would disappear.

Finally, this method is designed for 2D models, and has been developed to work at local distances (in the order of metres). For this reason, it could work very well in small urban and archaeological contexts.

**Acknowledgments.** This study is part of the oral contribution “Bayesian approach to the inversion of magnetic data for near-surface studies. Application to the archaeological site of San Pietro Infine (southern Italy)”, by R. Salone, S. Tarantino, L. Spagnuolo, A. Frisetti, M. La Manna, A. Emolo, R. Di Maio, presented at the 40th GNGTS National Conference, which was selected for submission to the Bulletin of Geophysics and Oceanography. In this regard, the GNGTS scientific committee is gratefully acknowledged. We also thank the editor, Dario Slejko, and two anonymous reviewers for their useful comments and suggestions, which were very helpful in improving the manuscript. The inversion code has been implemented in Matlab (R2022a release). All figures have been realised by using Matlab.

## REFERENCES

- Abdelrahman E.M., El-Araby T.M. and Essa K.S.; 2003a: *A least-squares minimisation approach to depth, index parameter, and amplitude coefficient determination from magnetic anomalies due to thin dykes*. Explor. Geophys., 34, 241-248.
- Abdelrahman E.M., El-Arby H.M., El-Arby T.M. and Essa K.S.; 2003b: *A least-squares minimization approach to depth determination from magnetic data*. Pure Appl. Geophys., 160, 1259-1271.
- Ai H., Essa K.S., Ekinci Y.L., Balkaya Ç., Li H. and Géraud Y.; 2022: *Magnetic anomaly inversion through the novel barnacles mating optimization algorithm*. Sci. Rep., 12, 22578, 28 pp., doi: 10.1038/s41598-022-26265-0.
- Asfahani J. and Tlas M.; 2007: *A robust nonlinear inversion for the interpretation of magnetic anomalies caused by faults, thin dikes and spheres like structure using stochastic algorithms*. Pure Appl. Geophys., 164, 2023-2042.
- Aster R.C., Borchers B. and Thurber C.H.; 2018: *Parameter estimation and inverse problems, 3rd ed.* Elsevier, Amsterdam, The Netherlands, 404 pp.
- Beardsmore G., Durrant-Whyte H., McCalman L., O’Callaghan S. and Reid A.; 2016: *A Bayesian inference tool for geophysical joint inversions*. ASEG Extended Abstracts, 2016, 1-10, doi: 10.1071/ASEG2016ab131.
- Biswas A.; 2018: *Inversion of source parameters from magnetic anomalies for mineral/ore deposits exploration using global optimization technique and analysis of uncertainty*. Nat. Resour. Res., 27, 77-107
- Biswas A. and Acharya T.; 2016: *A very fast simulated annealing method for inversion of magnetic anomaly over semi-infinite vertical rod-type structure*. Model. Earth Syst. Environ., 2, 1-10, doi: 10.1007/s40808-016-0256-x.
- Di Maio R., La Manna M. and Piegari E.; 2016: *3D reconstruction of buried structures from magnetic, electromagnetic and ERT data: example from the archaeological site of Phaistos (Crete, Greece)*. Archaeolog. Prospect., 23, 287-299.
- Di Maio R., Milano L. and Piegari E.; 2020: *Modeling of magnetic anomalies generated by simple geological structures through Genetic-Price inversion algorithm*. Phys. Earth Planet. Inter., 305, 106520, 12 pp., doi: 10.1016/j.pepi.2020.106520.

- Di Maio R., Emolo A., Frisetti A., Abate N., La Manna M., Pierri I., Salone R. and Tarantino S.; 2023: *Reconstruction of archaeological contexts through the integrated use of airborne LiDAR and geophysical survey: the case study of San Pietro Infine (Caserta, southern Italy)*. J. Archaeolog. Sci., R, 49, 104013, 16 pp., doi: 10.1016/j.jasrep.2023.104013.
- Essa K.S. and Elhussein M.; 2018: *PSO (Particle Swarm Optimization) for interpretation of magnetic anomalies caused by simple geometrical structures*. Pure Appl. Geophys., 175, 3539-3553.
- Essa K.S. and Elhussein M.; 2019: *Magnetic interpretation utilizing a new inverse algorithm for assessing the parameters of buried inclined dike-like geological structure*. Acta Geophys., 67, 533-544.
- Essa K.S. and Elhussein M.; 2020: *Interpretation of magnetic data through particle swarm optimization: mineral exploration cases studies*. Nat. Resour. Res., 29, 521-537, doi: 10.1007/s11053-020-09617-3.
- Essa K.S. and Diab Z.E.; 2022: *An automatic inversion approach for magnetic data applying the global bat optimization algorithm (GBOA): application to ore deposits and basement rock intrusion*. Geomech. Geophys. Geo-Energ. Geo-Resour., 8, 185, 22 pp., doi: 10.1007/s40948-022-00492-1.
- Essa K.S., Mehane S. and Elhussein M.; 2021: *Magnetic data profiles interpretation for mineralized buried structures identification applying the variance analysis method*. Pure Appl. Geophys., 178, 973-993.
- Fassbinder J.W.E.; 2017: *Magnetometry for Archaeology*. In: Gilbert A.S. (ed.), Encyclopedia of Geoarchaeology, Encyclopedia of Earth Sciences Series, Springer, Dordrecht, The Netherlands, pp. 499-514, doi: 10.1007/978-1-4020-4409-0\_169.
- Göktürkler G. and Balkaya Ç.; 2012: *Inversion of self-potential anomalies caused by simple-geometry bodies using global optimization algorithms*. J. Geophys. Eng., 9, 498-507.
- Güdük N., de la Varga M., Kaukolinnä J. and Wellmann F.; 2021: *Model-based probabilistic inversion using magnetic data: a case study on the Kevitsa deposit*. Geosci., 11, 150, 19 pp., doi: 10.3390/geosciences11040150.
- Ma G., Liu C., Xu J. and Meng Q.; 2017: *Correlation imaging method based on local wavenumber for interpreting magnetic data*. J. Appl. Geophys., 138, 17-22.
- Mehane S., Essa K.S. and Diab Z.E.; 2021: *Magnetic data interpretation using a new R-parameter imaging method with application to mineral exploration*. Nat. Resour. Res., 30, 77-95.
- Olierook H.K.H., Scalzo R., Kohn D., Chandra R., Farahbakhsh E., Clark C., Reddy S.M.R. and Müller D.; 2021: *Bayesian geological and geophysical data fusion for the construction and uncertainty quantification of 3D geological models*. Geosci. Front., 12, 479-493, doi: 10.1016/j.gsf.2020.04.015.
- Parker R.L.; 1977: *Understanding inverse theory*. Annu. Rev. Earth Planet. Sci., 5, 35-64.
- Piro S., Samir A. and Versino L.; 1998: *Position and spatial orientation of magnetic bodies from archaeological magnetic surveys*. Ann. Geophys., 41, 343-358.
- Salone R., Tarantino S., Spagnuolo L., Frisetti A., La Manna M., Emolo A. and Di Maio R.; 2022: *Bayesian approach to the inversion of magnetic data for near-surface studies. Application to the archaeological site of San Pietro Infine (southern Italy)*. In: Proc. 40th Gruppo Nazionale di Geofisica della Terra Solida (NGGTS) National Congress, Trieste, Italy, 4 pp.
- Sambridge M.; 1999: *Geophysical inversion with a neighborhood algorithm—I. Searching a parameter space*. Geophys. J. Int., 138, 479-494, doi: 10.1046/j.1365-246X.1999.00876.x.
- Sambridge M. and Mosegaard K.; 2002: *Monte Carlo methods in geophysical inverse problems*. Rev. Geophys., 40, 3-29.
- Sampietro D., Capponi M. and Maurizio G.; 2022: *3D Bayesian inversion of potential fields: the Quebec Oka carbonatite complex case study*. Geosci., 12, 382, 16 pp., doi: 10.3390/geosciences12100382.
- Silliman S.W., Farnsworth P. and Lightfoot K.G.; 2000: *Magnetometer prospecting in historical archaeology: evaluating survey options at a 19th-century rancho site in California*. Hist. Archaeolog., 34, 89-109.
- Tarantola A.; 1987: *Inverse problem theory and methods for model parameter estimation, 1st ed.* Elsevier, Amsterdam, The Netherlands, 619 pp.
- Telford W.M., Geldart L.P. and Sheriff R.E.; 1991: *Applied Geophysics, 2nd ed.* Cambridge University Press, Cambridge, UK, 770 pp.
- Tlas M. and Asfahani J.; 2011: *Fair function minimization for interpretation of magnetic anomalies due to thin dikes, spheres and faults*. J. Appl. Geophys., 75, 237-243.

*Corresponding author:* Rosanna Salone  
 Dipartimento di Scienze della Terra, dell'Ambiente e delle Risorse, Università degli Studi di Napoli Federico II  
 Complesso Universitario di Monte S. Angelo, via Cintia 21, 80126 Napoli, Italy  
 Phone: +39 081 679299; e-mail: rosanna.salone@unina.it